Research Article | Vol. 27, No. 20 / 30 September 2019 / Optics Express 27737
Optics EXPRESS

Experimental characterization of the speckle pattern at the output of a multimode optical fiber

DONATUS HALPAAP,[1,2] JORDI TIANA-ALSINA,[1] MERITXELL VILASECA,[2] AND CRISTINA MASOLLER[1,*]

[1]Departament de Física, Universitat Politècnica de Catalunya, St. Nebridi 22, 08222 Terrassa, Barcelona, Spain
[2]Centre de Desenvolupament de Sensors, Instrumentació i Sistemes, Universitat Politècnica de Catalunya, St. Nebridi 10, 08222 Terrassa, Barcelona, Spain
*cristina.masoller@upc.edu

Abstract: Speckle patterns produced by coherent waves interfering with each other are undesirable in many imaging applications (for example, in laser projection systems) but on the other hand, they contain useful information that can be exploited (for example, for blood flow analysis or reconstruction of the object that generates the speckle). It is therefore important to understand how speckle can be enhanced or reduced by tailoring the coherence of laser light. Using a conventional semiconductor laser and a multimode optical fiber we study experimentally how the speckle pattern depends on the laser pump current and on the image acquisition settings. By varying the pump current from below to above the lasing threshold, and simultaneously tuning the image exposure time to compensate for the change in brightness, we find conditions that allow for recorded images with similar average intensity, but with speckle contrast (the standard deviation of the intensity over the average intensity) as low as 0.16, or as high as 0.99.

1. Introduction

Laser light is used for imaging techniques because it offers high brightness and beam directionality. In particular, semiconductor lasers are very popular because they are efficient, inexpensive and cover a wide range of wavelengths. However, when laser light with high spatial and temporal coherence is transmitted through or reflected by an object that is rough on the scale of the wavelength, scattered light interferes, which leads to a random distribution of light intensity, known as speckle pattern [1], which can reduce resolution or make imaging impossible.

Therefore, in microscopy, in laser projection, and in other systems that use coherent light sources, methods for speckle reduction or removal are employed, e.g. a rotating diffuser [2], illumination from different angles, with different polarizations, or with various wavelengths [1]. Other approaches for speckle reduction consist of employing screens made of microlenses [3] or utilizing the intermodal dispersion in long enough optical fibers [4–6].

Other applications use speckle to their advantage, e.g. for laser speckle contrast imaging in blood flow analysis [7], for recognizing scatterers [8], for realizing compact [9,10] and high-precision [11] spectrometers, for reconstructing the object from which speckle emerges [12], for imaging through scattering media [13–15] or around corners [16,17].

Our work is motivated by the problem of speckle reduction in double pass (DP) ocular imaging [18,19]. The DP technique offers an overall measurement of the optical quality of a patient's eye. It is based on determining the point spread function (PSF) of the eye by observing the reflection of a light point projected onto the retina in order to draw conclusions on aberrations and intraocular scattering. The ideal light source for this type of measurement should emit between green (for smallest amount of retinal scattering) and near-infrared (for patient comfort) [20–22] and should offer a highly directional beam that provides several tens of microwatts of power at the corneal surface. As speckle contrast increases when the spectral width of the source decreases

#371717 https://doi.org/10.1364/OE.27.027737
Journal © 2019 Received 11 Jul 2019; revised 7 Aug 2019; accepted 9 Aug 2019; published 17 Sep 2019

Optics EXPRESS

[1], to minimize speckle we seek to use a source with a relatively broad spectrum. In addition, it should be of low cost. A superluminiscent diode meets the other requirements [19,23], but its cost prevents its use in inexpensive DP instruments.

Alternative approaches for reducing speckle in DP imaging include the use of acoustic modulation of laser beams [24] or the periodic variation of the vergence of a lens in the light beam [25] (but these are not low cost solutions), or by mechanical means: employing a vibrating mirror for scanning the beam [26] is a low cost solution, but introduces undesired mechanical vibrations in the setup.

An all-optical approach for speckle reduction includes broadening the spectrum through optical feedback [27]; however, the broadening is limited by the gain bandwidth of the semiconductor material and is not sufficient to obtain a significant speckle reduction. Other approaches are based on the introduction of a disordered material in the laser cavity to facilitate multiple scattering [28], or the use of specially designed cavities [29,30] (see [31] for a recent review). The drawback of these approaches for use in DP imaging systems is that they are not commercially available.

An alternative strategy that we examine here is the possibility of controlling the amount of speckle produced by semiconductor laser light by tuning the laser pump current across the lasing threshold.

Below the threshold the emitted light is mainly due to spontaneous emission and thus of low coherence. When the pump current, J_p, is increased above the threshold, the emitted light becomes coherent due to stimulated emission and the linewidth of the spectrum decreases. A multimode fiber generates apparently random speckle patterns [29]. When a laser source is used with a spectrum that contains a large number of narrow longitudinal modes, patterns with high speckle contrast can be obtained [4,5]. Here we use a multimode semiconductor laser and a multimode fiber to generate speckle patterns and analyze how the amount of speckle depends on the laser current. Because below the threshold the intensity is very low, we also need to adjust the exposure time, t_{exp}. Thus, we vary (J_p, t_{exp}) in the range of values that permit to record images with sufficient intensity, but preventing overexposure.

Our goal is to find pairs (J_p, t_{exp}) that allow recording images with similar average intensity, but with different amount of speckle.

2. Experimental setup

Figure 1(a) describes the experimental setup. We use a semiconductor laser (HL6750MG Thorlabs, USA) with nominal wavelength λ = 685 nm, and threshold current of approximately 26.7 mA at 18.0 °C. Speckle is created by a step-index multimode fiber with a core diameter of 200 μm (M72L02, Thorlabs) by interference of different guided modes [4,29]. We record the intensity at the end of the fiber with a 8 bit CMOS camera (UI-1240SE-M, IDS, Germany). The laser pump current, J_p, and the exposure time, t_{exp}, are control parameters that are varied within the range of values that permit recording images whose brightness is not too low, nor overexposed. A neutral density filter (NDF) used during all measurements ensures that the shortest possible exposure time of the camera is sufficient to obtain non-overexposed images at high pump currents.

The amount of speckle is quantified by the speckle contrast, $C = \sigma_I/\langle I\rangle$, where σ_I is the standard deviation of the intensity and $\langle I\rangle$ is the mean intensity. To minimize the influence of the non-uniformity of the intensity distribution, we calculate C inside the circular central area of radius 200 pixels, as shown in Fig. 1(b), which encloses approximately 125000 pixels with values in the range [0-255]. In this way, we disregard the outer part of the image. We have verified that the results are robust to the size of the area: a similar variation of C with the laser pump current and with the camera exposure time was found when considering radius of 150 or 250 pixels. We ensure that the size of the imaged speckle spots is larger than several camera pixels in order to avoid pixel averaging [3].

Optics EXPRESS

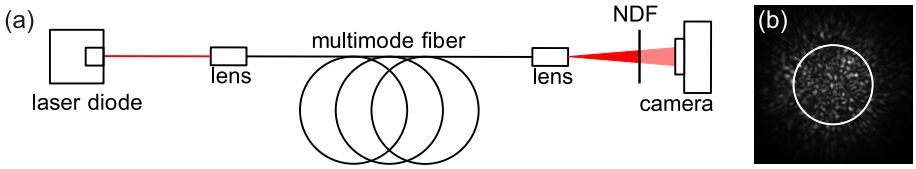

Fig. 1. (a) Experimental setup. NDF: neutral density filter of optical density 1.7. (b) Example speckle image with the area where the speckle contrast is computed indicated with a white circle.

3. Results

First we examine the optical spectra (measured with a 4 nm spectral resolution PR655 spectrometer, Photoresearch, USA) of the laser when it is pumped at various pump currents from below to above threshold, as shown in Fig. 2(a). Below threshold, the estimated linewidth (full width half maximum) is about 19 nm (see inset). In Fig. 2(b) we show in color code the spectrum of the laser (measured with an optical spectrum analyzer, MS9710C, Anritsu, Japan), as a function of the pump current. We see that above the threshold several cavity modes turn on (yellow lines) and the emission becomes nearly monomode at higher pump currents.

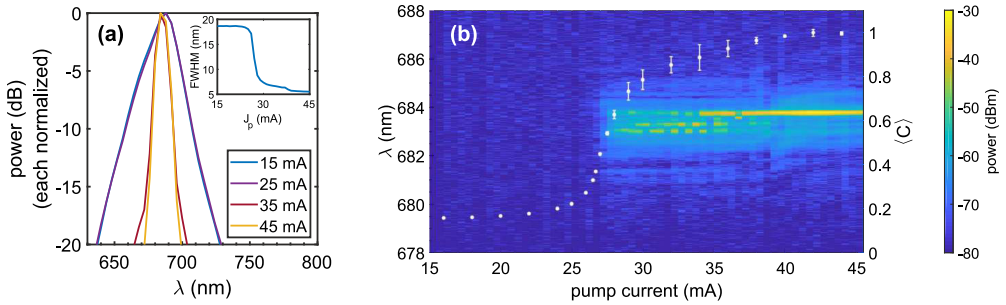

Fig. 2. (a) Optical spectra recorded at various pump currents (J_p = 15 mA, 25 mA, 35 mA, 45 mA), normalized to the maximum value. The spectra of 15 mA and 25 mA are almost indistinguishable. The inset shows the relationship between pump current and linewidth (full width half maximum). (b) Optical spectrum in color code vs. the pump current. The white dots represent the speckle contrast, averaged over measurements performed with different exposure times. The error bars indicate one standard deviation.

We recorded images of speckle patterns at pump currents from J_p = 16 mA (below the lasing threshold) up to 44 mA (single-mode emission) using different exposure times for each pump current value (for most pump currents, at least five images with different exposure times were taken). The criterion used to determine the range of exposure times is the same for all pump currents: we selected t_{exp} such that the images were neither overexposed (i.e. had no pixel with the maximum digital value of 255), nor of very low brightness (we disregarded images where the pixels within the circle had an average digital value < 10 in order to avoid quantization effects and possible dominance of noise).

The white dots on top of the spectral map, Fig. 2(b), represent the mean speckle contrast, $\langle C \rangle$, averaged over the speckle contrast from images obtained with different exposure times, and the error bars represent one standard deviation. We see that below $J_p \approx 24$ mA $\langle C \rangle$ is small ($\langle C \rangle \approx 0.16$) and only slightly increases with the pump current. Between $J_p \approx 24$ mA and 30 mA, coinciding with the lasing threshold, $\langle C \rangle$ increases strongly, whereupon the increase flattens and reaches a plateau of $\langle C \rangle \approx 1$ at 42 mA. The increase of C does not happen instantaneously

Optics EXPRESS

when tuning the pump current from below to above threshold because first several modes start lasing before the output changes to single-mode at around $J_p \approx 40$ mA. The variation of the speckle contrast for images taken with different exposure times (represented by the error bars in Fig. 2(b)) is negligible at low and high pump currents. However, for an intermediate range of pump currents (29 mA<J_p<40 mA), there is more variability (larger error bars), which we attribute to the competition of the laser cavity modes, which create different realizations of speckle patterns for the same pump current. The shape of the plot of C vs J_p in log-log scale (not shown) is similar to the input-output characteristic of the laser, but does not show the same saturation behavior at low pump currents, perhaps due to the limited sensitivity of the camera

Figure 3 shows the speckle contrast computed from all the individual images recorded, as a function of the mean intensity of the image. In Fig. 3(a), the color indicates the value of the pump current, in Fig. 3(b), the exposure time. The highest mean intensities correspond to low speckle contrast values, i.e., relatively homogeneous patterns that originate from low coherence light at pump currents under the lasing threshold, which are recorded with a relatively long exposure times of the camera ($t_{exp} = 5 - 60$ ms). At lower mean intensities, a large range of speckle contrasts can be achieved for a constant mean intensity by adjusting both the pump current and the exposure time. The highest speckle contrast values ($C \approx 1$) occur for $\langle I \rangle$<30.

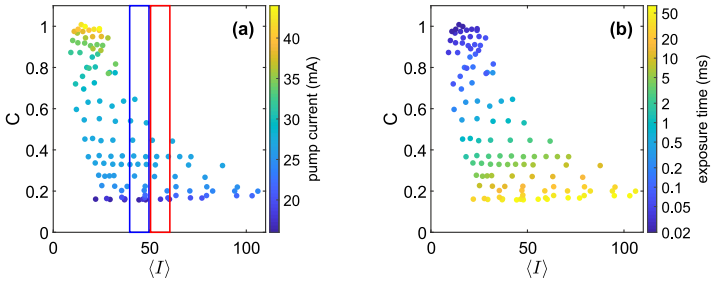

Fig. 3. Speckle contrast as a function of the mean intensity (in digital levels) for the same data as shown in Fig. 2(b). In (a), the color represents the corresponding pump current; in (b), it shows the exposure time.

In Fig. 4, we present six example images recorded with different pump currents and exposure times, and the corresponding intensity histograms, obtained from the pixel values within the circle. In the first two lines, from top to bottom, the mean intensities of the speckle patterns lie within ranges of $\langle I \rangle \in [40, 50]$ and $\langle I \rangle \in [50, 60]$, respectively. The speckle patterns recorded with the laser current above the threshold (right column) use the full dynamic range of the camera (8 bit, 256 digital gray values). Patterns with approximately the same mean intensity, but taken with the pump current below the threshold (left column) and with much longer exposure times are more homogeneous, i.e., have a narrower intensity histogram, and thus lower speckle contrast. In the bottom line of Fig. 4, we present the speckle pattern with the highest mean intensity, $\langle I \rangle = 106$ and that with highest speckle contrast, $C = 0.99$, obtained with a pump current of $J_p = 44$ mA.

The two panels in Fig. 5 show the values of (J_p, t_{exp}) used for each speckle measurement. In Fig. 5(a), the color of each point represents the mean intensity of the speckle pattern, while in Fig. 5(b), the color represents the speckle contrast. We note that, in order to obtain well-exposed images, t_{exp} needs to be decreased by three orders of magnitude (from $t_{exp} = 60$ ms to 0.03 ms) when the pump current is increased from $J_p = 16$ mA to 44 mA. As it was shown in Fig. 3, the highest mean intensities and the lowest speckle contrasts are achieved below the lasing threshold with long exposure times.

Optics EXPRESS

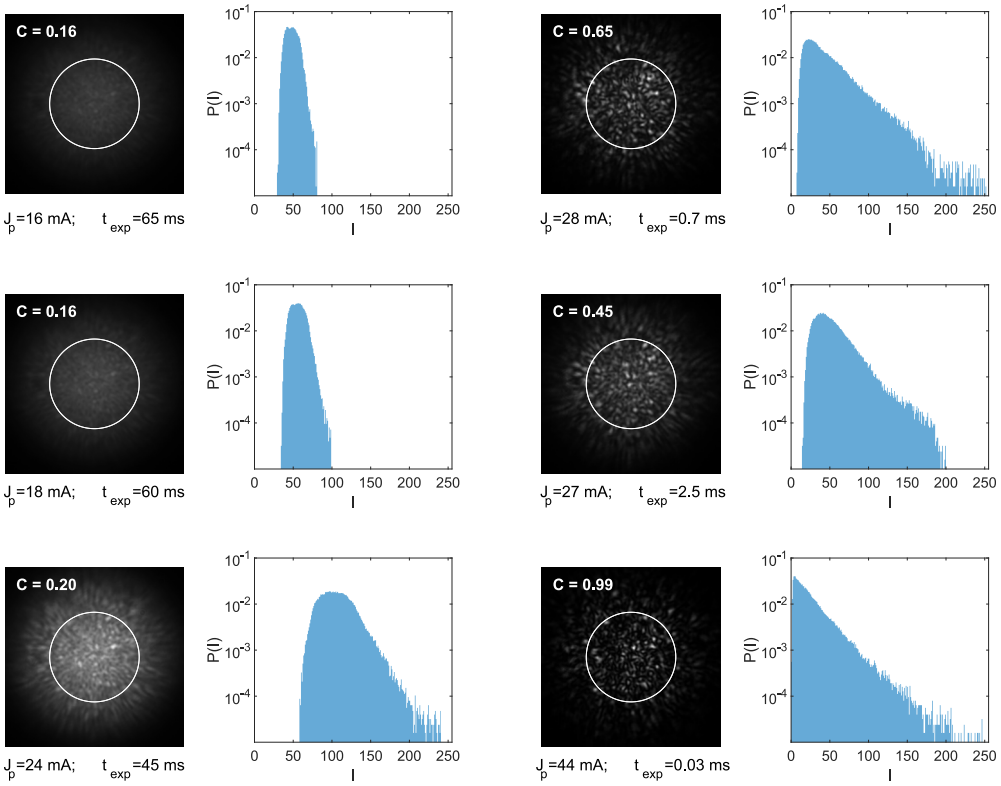

Fig. 4. Example images and histograms depicting the intensity distribution inside the areas indicated by white circles. In the first two lines from top to bottom, we present images of similar average intensities, within $\langle I \rangle \in [40, 50]$, and $\langle I \rangle \in [50, 60]$, respectively, from low (left column) and high pump current (right column), taken with different exposure times. In the third line, the cases of highest mean intensity ($\langle I \rangle \approx 106$, left column) and highest speckle contrast ($C = 0.99$ and $\langle I \rangle \approx 24$, right column) are shown.

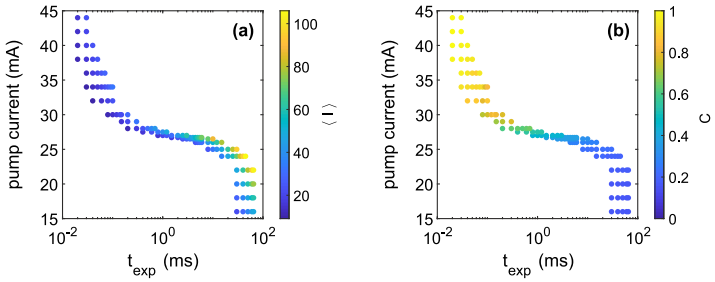

Fig. 5. Scatter plot of the exposure time and the pump current for all measurements. The color code indicates (a) the mean intensity, (b) the speckle contrast.

Optics EXPRESS

In Fig. 6, we show for two different intervals of mean intensities, corresponding to vertical windows in Fig. 3(a), $\langle I \rangle \in [40, 50]$ (blue window) and $\langle I \rangle \in [50, 60]$ (red window), the plots of t_{exp} vs. J_{p}. The color code indicates the speckle contrast and shows that different C values that can be achieved by adjusting t_{exp} and J_{p}. The first four images shown in Fig. 4 correspond to the lowest and highest pump currents in each of these plots.

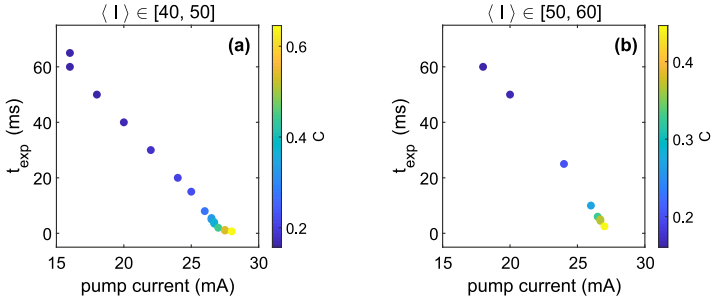

Fig. 6. Exposure time vs pump current for images that have mean intensity in the range (a) $\langle I \rangle \in [40, 50]$ and (b) $\langle I \rangle \in [50, 60]$. The color code indicates the speckle contrast.

4. Conclusions and discussion

We have studied experimentally how the speckle pattern at the output of a multimode fiber depends on the laser pump current and on the image acquisition settings. We have obtained images of speckle patterns with different amount of speckle (speckle contrast $C \approx 0.16 - 0.99$) by tuning the pump current from below the lasing threshold to above the threshold, $J_{\text{p}} = 16$ mA to 44 mA, and we kept the average intensity of the images within an appropriate range of values (to avoid too dark images or overexposed images) by adjusting the exposure time of the camera over three orders of magnitude, from $t_{\text{exp}} = 60$ ms to 0.02 ms. We have observed a sharp increase in the speckle contrast when the pump current is varied from below to above the threshold. This observation is interesting for applications where speckle needs to be suppressed or enhanced. In particular, if high intensity illumination is not required, or if long exposure times are possible, lowering the pump current under the threshold can be a simple solution for adjusting the amount of speckle.

For speckle reduction in DP imaging, a laser offering higher output power below threshold would be needed. When the laser in our setup is pumped just below the threshold ($J_{\text{p}} = 24$ mA), it produces an output of 80 microwatts. On the corneal plane, the maximum permissible exposure is a few tens of microwatts, depending on the wavelength. However, due to the optics necessary for improving the beam quality and guiding the light to the eye, only a small fraction of the power from the laser diode will arrive at the eye. Images taken with low power require longer exposure times, which reduces image quality because of unavoidable eye movements of patients.

In future work, it will be interesting to study, as a low-cost all-optical solution for speckle reduction, the possibility of combining the effects of optical perturbations (such as optical feedback that generates chaotic light) with a long multimode optical fiber. The use of optical feedback alone results in a reduction of speckle [27]. Particularly promising is the so-called coherence collapse regime, characterized by an abrupt increase of the line width [32,33]. Furthermore, sending the chaotic beam through a long enough multimode fiber can produce a more significant reduction, due to modal dispersion [4–6].

Optics EXPRESS

Funding

European Commission (675512); Ministerio de Economía y Competitividad (DPI2017-89414-R, PGC2018-099443-B-I00); Institució Catalana de Recerca i Estudis Avançats (academia).

References

1. J. W. Goodman, *Speckle Phenomena in Optics: Theory and Applications* (Roberts & Company, 2007).
2. T. Stangner, H. Zhang, T. Dahlberg, K. Wiklund, and M. Andersson, "Step-by-step guide to reduce spatial coherence of laser light using a rotating ground glass diffuser," Appl. Opt. **56**(19), 5427–5435 (2017).
3. J. Pauwels and G. Verschaffelt, "Speckle reduction in laser projection using microlens-array screens," Opt. Express **25**(4), 3180–3195 (2017).
4. M. Imai and Y. Ohtsuka, "Speckle-pattern contrast of semiconductor laser propagating in a multimode optical fiber," Opt. Commun. **33**(1), 4–8 (1980).
5. R. Dandliker, A. Bertholds, and F. Maystre, "How modal noise in multimode fibers depends on source spectrum and fiber dispersion," J. Lightwave Technol. **3**(1), 7–12 (1985).
6. J. G. Manni and J. W. Goodman, "Versatile method for achieving 1% speckle contrast in large-venue laser projection displays using a stationary multimode optical fiber," Opt. Express **20**(10), 11288–11315 (2012).
7. D. A. Boas and A. K. Dunn, "Laser speckle contrast imaging in biomedical optics," J. Biomed. Opt. **15**(1), 011109 (2010).
8. E. Valent and Y. Silberberg, "Scatterer recognition via analysis of speckle patterns," Optica **5**(2), 204–207 (2018).
9. B. Redding, S. M. Popoff, and H. Cao, "All-fiber spectrometer based on speckle pattern reconstruction," Opt. Express **21**(5), 6584–6600 (2013).
10. B. Redding, S. F. Liew, R. Sarma, and H. Cao, "Compact spectrometer based on a disordered photonic chip," Nat. Photonics **7**(9), 746–751 (2013).
11. G. D. Bruce, L. O'Donnell, M. Chen, and K. Dholakia, "Overcoming the speckle correlation limit to achieve a fiber wavemeter with attometer resolution," Opt. Lett. **44**(6), 1367–1370 (2019).
12. P. S. Idell, J. R. Fienup, and R. S. Goodman, "Image synthesis from nonimaged laser-speckle patterns," Opt. Lett. **12**(11), 858–860 (1987).
13. J. Bertolotti, E. G. van Putten, C. Blum, A. Lagendijk, W. L. Vos, and A. P. Mosk, "Non-invasive imaging through opaque scattering layers," Nature **491**(7423), 232–234 (2012).
14. E. Edrei and G. Scarcelli, "Memory-effect based deconvolution microscopy for super-resolution imaging through scattering media," Sci. Rep. **6**(1), 33558 (2016).
15. E. Edrei and G. Scarcelli, "Optical imaging through dynamic turbid media using the fourier-domain shower-curtain effect," Optica **3**(1), 71–74 (2016).
16. O. Katz, E. Small, and Y. Silberberg, "Looking around corners and through thin turbid layers in real time with scattered incoherent light," Nat. Photonics **6**(8), 549–553 (2012).
17. O. Katz, P. Heidmann, M. Fink, and S. Gigan, "Non-invasive single-shot imaging through scattering layers and around corners via speckle correlations," Nat. Photonics **8**(10), 784–790 (2014).
18. J. Santamaría, P. Artal, and J. Bescós, "Determination of the point-spread function of human eyes using a hybrid optical–digital method," J. Opt. Soc. Am. A **4**(6), 1109–1114 (1987).
19. D. Halpaap, C. E. García-Guerra, M. Vilaseca, and C. Masoller, "Speckle reduction in double-pass retinal images," Sci. Rep. **9**(1), 4469 (2019).
20. N. López-Gil and P. Artal, "Comparison of double-pass estimates of the retinal-image quality obtained with green and near-infrared light," J. Opt. Soc. Am. A **14**(5), 961–971 (1997).
21. M. Vilaseca and J. Pujol, "Response to the letter to the editor by dr van den berg," Aust. J. Optom. **94**(4), 393–395 (2011).
22. J. A. Martínez-Roda, M. Vilaseca, J. C. Ondategui, A. Giner, F. J. Burgos, G. Cardona, and J. Pujol, "Optical quality and intraocular scattering in a healthy young population," Aust. J. Optom. **94**(2), 223–229 (2011).
23. F. Sanabria, M. A. Arévalo, F. Díaz-Doutón, C. E. García-Guerra, and J. P. Ramo, "Technical improvements applied to a double-pass setup for performance and cost optimization," Opt. Eng. **53**(6), 061710 (2014).
24. V. Albanis, E. N. Ribak, and Y. Carmon, "Reduction of speckles in retinal reflection," Appl. Phys. Lett. **91**(5), 054104 (2007).
25. C. García-Guerra, M. Aldaba, M. Arjona, and J. Pujol, "Speckle reduction in double-pass retinal images using variable-focus lenses," J. Eur. Opt. Soc. Rapid Publ. **10**, 15001 (2015).
26. H. Hofer, P. Artal, B. Singer, J. L. Aragón, and D. R. Williams, "Dynamics of the eye's wave aberration," J. Opt. Soc. Am. A **18**(3), 497–506 (2001).
27. B. Dingel and S. Kawata, "Speckle-free image in a laser-diode microscope by using the optical feedback effect," Opt. Lett. **18**(7), 549–551 (1993).
28. B. Redding, M. A. Choma, and H. Cao, "Speckle-free laser imaging using random laser illumination," Nat. Photonics **6**(6), 355–359 (2012).
29. B. Redding, A. Cerjan, X. Huang, M. L. Lee, A. D. Stone, M. A. Choma, and H. Cao, "Low spatial coherence electrically pumped semiconductor laser for speckle-free full-field imaging," Proc. Natl. Acad. Sci. U. S. A. **112**(5), 1304–1309 (2015).

Optics EXPRESS

30. K. Kim, S. Bittner, Y. Zeng, S. Fatt Liew, Q. Wang, and H. Cao, "Electrically pumped semiconductor laser with low spatial coherence and directional emission," arXiv e-prints arXiv:1905.03671 (2019).
31. H. Cao, R. Chriki, S. Bittner, A. A. Friesem, and N. Davidson, "Complex lasers with controllable coherence," Nat. Rev. Phys. **1**(2), 156–168 (2019).
32. D. Lenstra, B. Verbeek, and A. Den Boef, "Coherence collapse in single-mode semiconductor lasers due to optical feedback," IEEE J. Quantum Electron. **21**(6), 674–679 (1985).
33. M. Sciamanna and K. A. Shore, "Physics and applications of laser diode chaos," Nat. Photonics **9**(3), 151–162 (2015).